



Evidence for WZ and ZZ production in final states with b -tagged jets

The DØ Collaboration
URL <http://www-d0.fnal.gov>
(Dated: November 15, 2011)

We present evidence for the combined production of VZ ($V = W$ or Z) events in final states containing charged leptons (electrons or muons) or neutrinos, and heavy flavor jets, using data collected by the DØ detector at the Fermilab Tevatron Collider. The analyzed samples correspond to 7.5 to 8.4 fb^{-1} of $p\bar{p}$ collisions at $\sqrt{s} = 1.96$ TeV. Assuming the ratio of the production cross sections $\sigma(WZ)$ and $\sigma(ZZ)$ as predicted by the standard model, we measure the total VZ cross section to be $\sigma(VZ) = 5.0 \pm 1.0$ (stat) $_{-1.2}^{+1.3}$ (syst) pb. This corresponds to a significance of 3.3 standard deviations above the background only hypothesis. Furthermore, we have separately measured the cross sections for the WZ and ZZ processes to be $\sigma(WZ) = 5.9 \pm 1.4$ (stat) ± 0.7 (syst) pb and $\sigma(ZZ) = 0.45 \pm 0.61$ (stat) ± 1.2 (syst) pb, in agreement with the standard model prediction.

Preliminary Results for the HCP 2011 Conference

I. INTRODUCTION

The production of VV ($V = W, Z$) boson pairs provides an important test of the electroweak sector of the standard model (SM). In $p\bar{p}$ collisions at $\sqrt{s} = 1.96$ TeV, the next-to-leading order (NLO) SM cross sections for these processes are $\sigma(WW) = 11.3 \pm 0.8$ pb, $\sigma(WZ) = 3.2 \pm 0.2$ pb and $\sigma(ZZ) = 1.2 \pm 0.1$ pb [1]. Measuring a significant departure in cross section or deviations in the predicted kinematic distributions would indicate the presence of anomalous gauge boson couplings [2] or new particles in extensions of the SM [3]. The VV production in $p\bar{p}$ collisions at the Fermilab Tevatron Collider has been observed in fully leptonic decay modes [4] and in semi-leptonic decay modes [5], where the combined $WW + WZ$ cross section was measured.

In this note we report evidence of WZ and ZZ production in final states where one of the Z boson decays to $b\bar{b}$ (although there is some signal contribution from $W \rightarrow c\bar{s}$, $Z \rightarrow c\bar{c}$) and the other weak boson decays to charged leptons or neutrinos ($W \rightarrow \ell\nu$, $Z \rightarrow \nu\nu$, or $Z \rightarrow \ell\ell$, with $\ell = e, \mu$). This analysis is also relevant as a proving ground for the searches for a low-mass Higgs boson produced in association with a weak boson and decaying into a $b\bar{b}$ pair [6], which share the exact same selection criteria and analysis techniques.

II. SUMMARY OF CONTRIBUTING ANALYSES

This result is the combination of three analyses [7–9] outlined in Table I. These analyses utilize data corresponding to integrated luminosities ranging from 7.5 to 8.4 fb^{-1} , collected by the D0 detector [10] at the Fermilab Tevatron Collider. They are organized into multiple sub-channels for different configurations of final state particles. To facilitate proper combination of signals, the analyses were constructed to use mutually exclusive event selections.

In the $\ell\nu b\bar{b}$ analysis [7], events containing an isolated electron or muon, and two or three jets are selected. The presence of a neutrino from the W decay is inferred from a large imbalance of transverse momentum (\cancel{E}_T). The $\nu\nu b\bar{b}$ analysis [8] selects events containing large \cancel{E}_T and exactly two jets. Finally, in the $\ell\ell b\bar{b}$ analysis [9], events are required to contain two electrons or two muons and at least two jets. In the $\ell\nu b\bar{b}$ and $\ell\ell b\bar{b}$ analyses, each lepton flavor of the W/Z boson decay ($\ell = e, \mu$) is treated as an independent channel. To ensure that the samples for the different analyses do not overlap, the $\ell\nu b\bar{b}$ analysis rejects events in which a second isolated electron or muon is identified, and the $\nu\nu b\bar{b}$ analysis rejects events in which any isolated electrons or muons are identified.

To isolate the $Z \rightarrow b\bar{b}$ decays, an algorithm for identifying jets consistent with the decay of a heavy-flavor quark is applied to each jet (b -tagging). Several kinematic variables sensitive to displaced decay vertices and jet tracks with large transverse impact parameters relative to the hard-scatter vertices are combined in a b -tagging discriminant based on boosted decision trees. This algorithm is an upgraded version of the neural network b -tagging tool used previously [11]. By adjusting the minimum requirement on the b -tagging output, a spectrum of increasingly stringent b -tagging operating points is achieved. Each of the analyses is separated into two groups: a double-tag (DT) group in which two of the jets are b -tagged with a loose tag requirement ($\ell\nu b\bar{b}$ and $\nu\nu b\bar{b}$) or one loose and one tight tag requirement ($\ell\ell b\bar{b}$); and an orthogonal single-tag (ST) group in which only one jet has a loose ($\ell\nu b\bar{b}$ and $\nu\nu b\bar{b}$) or tight ($\ell\ell b\bar{b}$) b -tag. A typical per-jet efficiency and fake rate for the loose (tight) b -tag selection is about 80% (50%) and 10% (0.5%), respectively. The corresponding efficiency for jets from c -quarks is 45% (12%). Furthermore, the $\ell\nu b\bar{b}$ and $\nu\nu b\bar{b}$ analyses use the output from the b -tagging algorithm as input to final discriminants. The signal in the DT sample is mainly composed of events with $Z \rightarrow b\bar{b}$ decays with smaller contributions from $Z \rightarrow c\bar{c}$ and $W \rightarrow c\bar{s}$ decays. In the ST sample, which places a much less stringent requirement on the b -jet content of the event, the contributions from the three decay modes are comparable. All three analyses use multivariate discriminants (MVA) based on decision trees as the final variables for extracting the VZ signal from the backgrounds.

The backgrounds from multijet production are measured from control samples in the data. The other backgrounds are generated by ALPGEN [12] and COMPHEP [13], with PYTHIA [14] providing parton-showering and hadronization. The primary background is from W/Z +jets, and is modeled with ALPGEN. The $\ell\nu b\bar{b}$ and $\ell\ell b\bar{b}$ analyses normalize these background to the data, whereas the $\nu\nu b\bar{b}$ analysis normalizes them to the prediction from ALPGEN. The

TABLE I: List of analysis channels and their corresponding integrated luminosities. See Sect. II for details ($\ell = e, \mu$).

Channel	Luminosity (fb^{-1})	Reference
$\ell\nu b\bar{b}$, ST/DT, 2/3 jets	7.5	[7]
$\nu\nu b\bar{b}$, ST/DT 2 jets	8.4	[8]
$\ell\ell b\bar{b}$, ST/DT ≥ 2 jets	7.5	[9]

fraction of the W/Z +jets in which the jets arise from heavy quarks (b or c) is obtained from NLO calculations using MCFM [15]. The background from $t\bar{t}$ events is normalized to the approximate NNLO cross section [16]. The s -channel and t -channel cross sections for the production of single-top quarks are from approximate NNLO+NNLL calculations [17] and approximate NNNLO+NLL calculations [18], respectively. The background from WW events is normalized to NLO calculations from MCFM [1].

III. SYSTEMATIC UNCERTAINTIES

The main sources of systematic uncertainty varies between the different analyses [7–9]. Here we summarize only the largest contributions. The $\nu\nu b\bar{b}$ and $\ell\nu b\bar{b}$ analyses carry an uncertainty on the integrated luminosity of 6.1% [19], while the overall normalization of the $\ell b\bar{b}$ analysis is determined from the NNLO Z/γ^* cross section [20] in data events near the peak of $Z \rightarrow \ell\ell$ decays. The uncertainty from the identification and measurement of jets is $\sim 7\%$. The uncertainty arising from the b -tagging rate ranges from 1 to 10%. All analyses include uncertainties associated with lepton measurement and acceptances, which range from 1 to 9% depending on the final state. The largest contribution for all analyses is the theoretical uncertainty on the background cross sections at 7-20% depending on the analysis channel and specific background. The uncertainty on the expected multijet background is dominated by the statistics of the data sample from which it is estimated. In addition, the analyses incorporate shape-dependent uncertainties on the kinematics of the dominant backgrounds. These shapes are derived from the potential variations of the MVA distributions due to generator and background modeling uncertainties. Further details on the systematic uncertainties are given in Tables II-IV. All systematic uncertainties originating from a common source are held to be correlated, as detailed in Table V.

IV. MEASUREMENT OF THE $WZ + ZZ$ CROSS SECTION

The total VZ cross section is determined from a fit of the MVA distributions of the background and signal samples to the data. The ratio of the WZ and ZZ cross sections is fixed to its SM prediction. The production of WW events is considered as a background. This fit is performed simultaneously on the distributions in all sub-channels by minimizing a negative log likelihood ratio function with respect to the signal cross section and variations in the systematic uncertainties [21]. This function is constructed from terms for Poisson fluctuations in the data, and a Gaussian prior for each systematic uncertainty. The magnitude of the systematic uncertainties is effectively constrained by the regions of the MVA distribution with low signal over background ratio. Different uncertainties are assumed to be mutually independent, but those common to multiple sub-channels are assumed to be 100% correlated.

The combined fit for the total VZ cross section distributions yields $\sigma(VZ) = 5.0 \pm 1.0$ (stat) $^{+1.3}_{-1.2}$ (syst) pb. This measurement is consistent with the NLO SM prediction of $\sigma(VZ) = 4.4 \pm 0.3$ pb [1]. To visualize the sensitivity of the combined analysis, we calculate the signal over background (s/b) in each bin of the MVA distributions from the contributing analyses. Bins with similar s/b are then combined to produce a single distribution, shown in Figure 1. In Figure 2 we show the distributions of the invariant mass of the dijet system after adjusting the signal and background predictions according to the results of the fit. Figure 3 shows the background subtracted dijet mass distributions after the fit. Distributions of the MVA and dijet mass for the contributing analyses can be found in the Appendix.

We estimate the statistical significance of the measured VZ signal by performing the same measurement on an ensemble of pseudo-experiments drawn from the background only hypothesis. Figure 4 shows the distribution of cross sections obtained from the background only pseudo-experiments compared to the cross section measured from data. The significance is found to be 3.3 standard deviations (s.d.). The expected significance is 2.9. Also shown in Figure 4 is the distribution of cross sections obtained from pseudo-experiments drawn from the SM signal+background hypothesis. It is also interesting to compare the distributions of the negative log-likelihood ratio (LLR) test statistic [22] for the two hypotheses to the LLR observed in data. We display the results of this comparison in Figure 5.

We also perform the fit with the signal divided into its separate WZ and ZZ components, which are allowed to float independently. The result of this simultaneous fit of $\sigma(WZ)$ and $\sigma(ZZ)$ using the MVA output distributions is shown in Figure 6. It yields $\sigma(WZ) = 5.9 \pm 1.4$ (stat) ± 0.7 (syst) pb and $\sigma(ZZ) = 0.45 \pm 0.61$ (stat) ± 1.2 (syst) pb. These results are to be compared to the NLO predictions of $\sigma(WZ) = 3.2 \pm 0.2$ pb and $\sigma(ZZ) = 1.2 \pm 0.1$ pb.

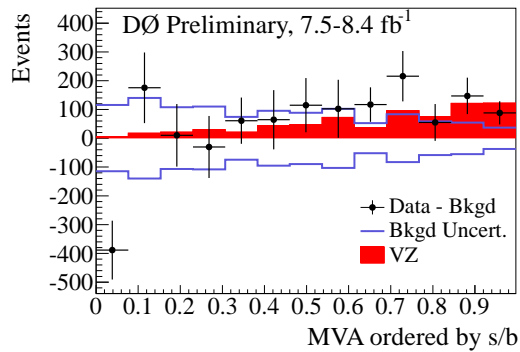


FIG. 1: Comparison of the measured VZ signal (filled histogram) to background-subtracted data (points). The background has been fit to the data in the hypothesis that both signal and background are present. Also shown is the ± 1 standard deviation uncertainty on the fitted background.

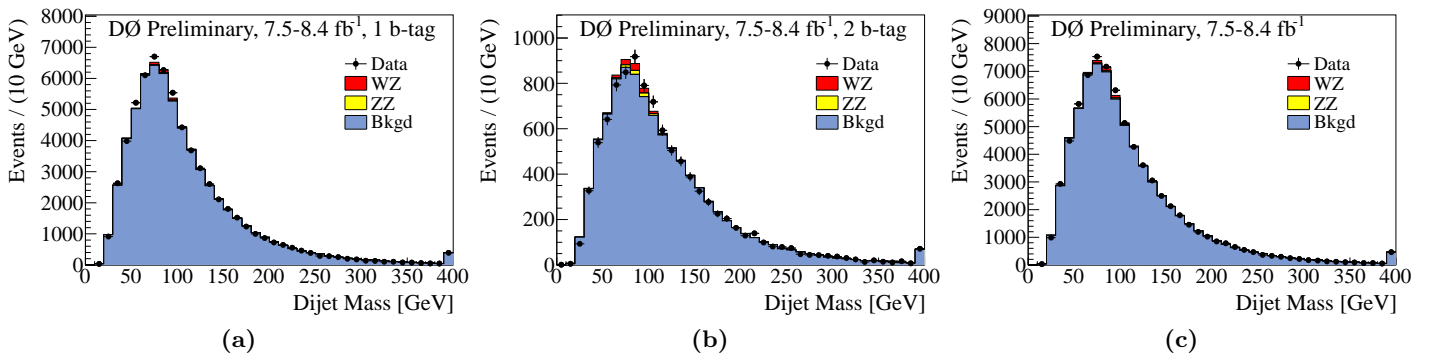


FIG. 2: Comparison of the fitted signal+background to data in the dijet mass distribution (summed over all channels) for the (a) ST, and (b) DT sub-channels; and (c) the sum of the ST and DT sub-channels. Events with a dijet mass greater than 400 GeV are included in the last bin of the distribution.

V. SUMMARY

In summary, we have combined analyses in the $\ell\nu b\bar{b}$, $\nu\nu b\bar{b}$, and $\ell\ell b\bar{b}$ ($\ell = e, \mu$) final states to obtain evidence with a significance of 3.3 s.d., for the production of VZ ($V = W$ or Z) events. The analyzed samples correspond to 7.5 to 8.4 fb^{-1} of $p\bar{p}$ collisions at $\sqrt{s} = 1.96$ TeV. We measure the total cross section for VZ production to be $\sigma(VZ) = 5.0 \pm 1.0$ (stat) $^{+1.3}_{-1.2}$ (syst) pb. Furthermore, we have separately measured the cross sections for the WZ and ZZ processes to be $\sigma(WZ) = 5.9 \pm 1.4$ (stat) ± 0.7 (syst) pb and $\sigma(ZZ) = 0.45 \pm 0.61$ (stat) ± 1.2 (syst) pb, in agreement with the SM predictions. These results demonstrate the ability of the D0 experiment to measure a signal containing two heavy-flavor jets in a background-dominated final state directly relevant to low mass Higgs searches.

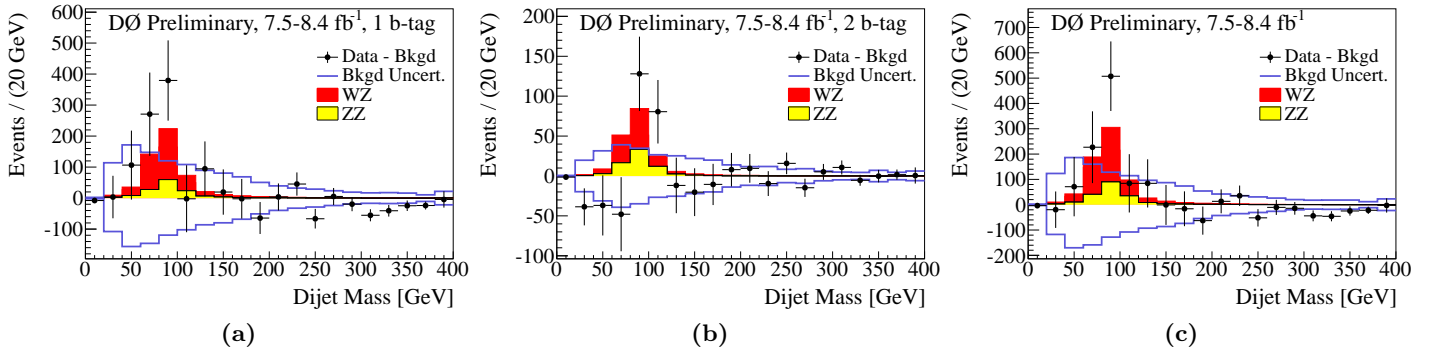


FIG. 3: Comparison of the measured WZ and ZZ signals (filled histograms) to background-subtracted data (points) in the dijet mass distribution (summed over all channels) for the (a) ST, and (b) DT sub-channels; and (c) the sum of the ST and DT sub-channels. Also shown is the ± 1 standard deviation uncertainty on the fitted background. Events with a dijet mass greater than 400 GeV are included in the last bin of the distribution.

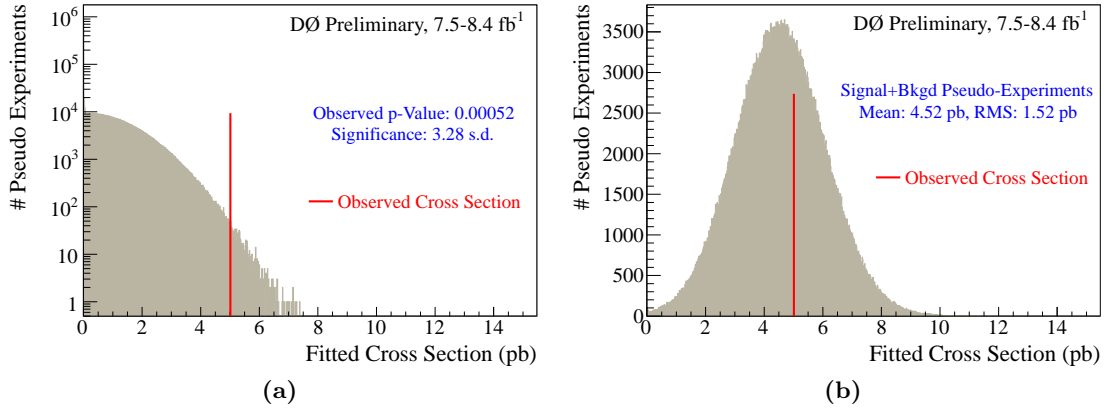


FIG. 4: Distribution of VZ cross sections obtained from (a) background-only pseudo-experiments and (b) signal+background pseudo-experiments. The observed cross section from the data (vertical red line) is also shown.

Acknowledgments

We thank the staffs at Fermilab and collaborating institutions, and acknowledge support from the DOE and NSF (USA); CEA and CNRS/IN2P3 (France); FASI, Rosatom and RFBR (Russia); CNPq, FAPERJ, FAPESP and FUNDUNESP (Brazil); DAE and DST (India); Colciencias (Colombia); CONACyT (Mexico); KRF and KOSEF

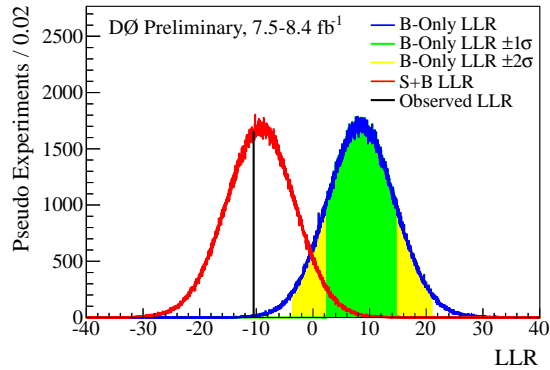


FIG. 5: LLR distributions obtained from background-only and signal+background pseudo-experiments compared to the LLR obtained from the data.

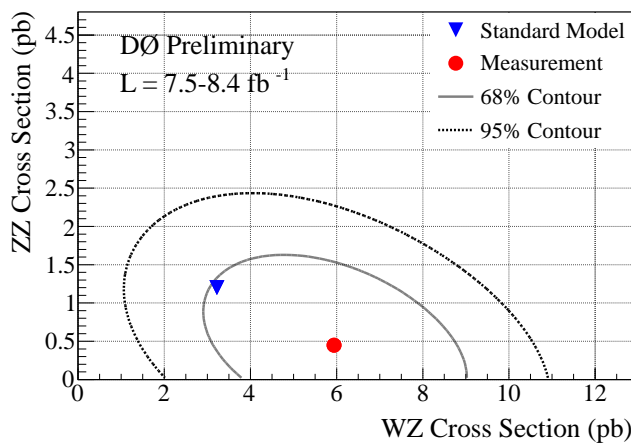


FIG. 6: Results from the simultaneous fit of $\sigma(WZ)$ and $\sigma(ZZ)$. The plot shows the best fit value with 68% and 95% uncertainty ellipses and the NLO SM prediction.

(Korea); CONICET and UBACyT (Argentina); FOM (The Netherlands); STFC and the Royal Society (United Kingdom); MSMT and GACR (Czech Republic); CRC Program and NSERC (Canada); BMBF and DFG (Germany); SFI (Ireland); The Swedish Research Council (Sweden); and CAS and CNSF (China).

-
- [1] J. M. Campbell and R. K. Ellis, Phys. Rev. D **60**, 113006 (1999) [arXiv:hep-ph/9905386].
 - [2] K. Hagiwara, S. Ishihara, R. Szalapski, and D. Zeppenfeld, Phys. Rev. D **48** (1993).
 - [3] J. C. Pati and A. Salam, Phys. Rev. D **10**, 275 (1974); **11** 703(E) (1975);
G. Altarelli, B. Mele, and M. Ruiz-Altaba, Z. Phys. C **45**, 109 (1989); **47**, 676(E) (1990);
L. Randall and R. Sundrum, Phys. Rev. Lett. **83**, 3370 (1999);
H. Davoudiasl, J. L. Hewett, and T. G. Rizzo, Phys. Rev. D **63**, 075004 (2001);
H. He *et al.*, Phys. Rev. D **78**, 031701 (2008).
 - [4] T. Aaltonen *et al.* (CDF Collaboration), Phys. Rev. Lett. **104**, 201801 (2010);
V. M. Abazov *et al.* (D0 Collaboration), Phys. Lett. B **695**, 67 (2011);
V. M. Abazov *et al.* (D0 Collaboration), Phys. Rev. D **84**, 011103 (2011).
 - [5] T. Aaltonen *et al.* (CDF Collaboration), Phys. Rev. Lett. **103**, 091803 (2009);
T. Aaltonen *et al.* (CDF Collaboration), Phys. Rev. Lett. **104**, 101801 (2010).
 - [6] V. M. Abazov *et al.* (D0 Collaboration), Phys. Rev. Lett. **104**, 071801 (2010);
V. M. Abazov *et al.* (D0 Collaboration), Phys. Rev. Lett. **105**, 251801 (2010);
V. M. Abazov *et al.* (D0 Collaboration), Phys. Lett. B **698**, 6 (2011).
 - [7] DØ Collaboration, DØ Note 6220-CONF (2011).
 - [8] DØ Collaboration, DØ Note 6223-CONF (2011).
 - [9] DØ Collaboration, DØ Note 6256-CONF (2011).
 - [10] DØ Collaboration, V. Abazov *et al.*, Nucl. Instrum. Meth. A **565**, 463 (2006) [arXiv:hep-ph/0507191].
 - [11] DØ Collaboration, V. Abazov *et al.*, Nucl. Instrum. Methods in Phys. Res. Sect. A **620**, 490 (2010) [arXiv:1002.4224].
 - [12] M. L. Mangano, M. Moretti, F. Piccinini, R. Pittau and A. D. Polosa, JHEP **0307**, 001 (2003). [arXiv:hep-ph/0206293].
 - [13] A. Pukhov *et al.*, arXiv:hep-ph/9908288 (1999).
 - [14] T. Sjöstrand, L. Lonnblad and S. Mrenna, arXiv:hep-ph/0108264.
 - [15] J. Campbell and R. K. Ellis, <http://mcfm.fnal.gov/>.
J. M. Campbell, R. K. Ellis, Nucl. Phys. Proc. Suppl. **205-206**, 10-15 (2010). [arXiv:1007.3492 [hep-ph]].
 - [16] U. Langenfeld, S. Moch and P. Uwer, Phys. Rev. D **80**, 054009 (2009) [arXiv:0906.5273 [hep-ph]].
 - [17] N. Kidonakis, arXiv:1005.3330 [hep-ph] (2010);
N. Kidonakis, Phys. Rev. D **81**, 054028 (2010).
 - [18] N. Kidonakis, Phys. Rev. D **74**, 114012 (2006) [arXiv:hep-ph/0609287].
 - [19] T. Andeen *et al.*, Report No. FERMILAB-TM-2365, 2007.
 - [20] R. Hamberg, W.L. van Neerven and W.B. Kilgore, Nucl Phys. **B359** 343 (1991), errata **B644** 403, hep-ph/0308087.
 - [21] W. Fisher, FERMILAB-TM-2386-E.
 - [22] T. Junk, Nucl. Instrum. Meth. A **434**, 435 (1999); A.Read, CERN 2000-005 (30 May 2000).

Appendix A: Additional Material

TABLE II: Systematic uncertainties for the $\ell\nu b\bar{b}$ single tag (ST) and double tag (DT) channels. Systematic uncertainties are listed by name; see the original references for a detailed explanation of their meaning and on how they are derived. Uncertainties are relative, in percent on the event yield. Shape uncertainties are labeled with an “(S)”, and “SO” represents uncertainties that affect only the shape, but not the event yield.

$\ell\nu b\bar{b}$ Single Tag (ST) channels relative uncertainties (%)

Contribution	Dibosons	$W + b\bar{b}/c\bar{c}$	$W+l.f.$	$t\bar{t}$	single top	Multijet
Luminosity	6.1	6.1	6.1	6.1	6.1	–
Electron ID/Trigger efficiency (S)	1–5	2–4	2–4	1–2	1–2	–
Muon Trigger efficiency (S)	1–3	1–2	1–3	2–5	2–3	–
Muon ID efficiency/resolution	4.1	4.1	4.1	4.1	4.1	–
Jet ID efficiency (S)	2–5	1–2	1–3	3–5	2–4	–
Jet Energy Resolution (S)	4–7	1–3	1–4	2–5	2–4	–
Jet Energy Scale (S)	4–7	2–5	2–5	2–5	2–4	–
Vertex Conf. Jet (S)	4–10	5–12	4–10	7–10	5–10	–
b -tag/taggability (S)	1–4	1–2	3–7	3–5	1–2	–
Heavy-Flavor K-factor	–	20	–	–	–	–
Multijet model, $\ell\nu b\bar{b}$ (S)	1–2	2–4	1–3	1–2	1–3	15
Multijet model, $\mu\nu b\bar{b}$	–	2.4	2.4	–	–	20
Cross Section	6	9	9	10	10	–
ALPGEN MLM pos/neg(S)	–	SO	–	–	–	–
ALPGEN Scale (S)	–	SO	SO	–	–	–
Underlying Event (S)	–	SO	–	–	–	–
PDF, reweighting	2	2	2	2	2	–

$\ell\nu b\bar{b}$ Double Tag (DT) channels relative uncertainties (%)

Contribution	Dibosons	$W + b\bar{b}/c\bar{c}$	$W+l.f.$	$t\bar{t}$	single top	Multijet
Luminosity	6.1	6.1	6.1	6.1	6.1	–
Electron ID/Trigger efficiency (S)	2–5	2–3	2–3	1–2	1–2	–
Muon Trigger efficiency (S)	2–4	1–2	1–2	2–4	1–3	–
Muon ID efficiency/resolution	4.1	4.1	4.1	4.1	4.1	–
Jet ID efficiency (S)	2–8	2–5	4–9	3–7	2–4	–
Jet Energy Resolution (S)	4–7	2–7	2–7	2–9	2–4	–
Jet Energy Scale (S)	4–7	2–6	2–7	2–6	2–7	–
Vertex Conf. Jet (S)	4–10	5–12	4–10	7–10	5–10	–
b -tag/taggability (S)	3–7	4–6	3–10	5–10	4–10	–
Heavy-Flavor K-factor	–	20	–	–	–	–
Multijet model, $\ell\nu b\bar{b}$ (S)	1–2	2–4	1–3	1–2	1–3	15
Multijet model, $\mu\nu b\bar{b}$	–	2.4	2.4	–	–	20
Cross Section	6	9	9	10	10	–
ALPGEN MLM pos/neg(S)	–	SO	–	–	–	–
ALPGEN Scale (S)	–	SO	SO	–	–	–
Underlying Event (S)	–	SO	–	–	–	–
PDF, reweighting	2	2	2	2	2	–

TABLE III: Systematic uncertainties for the $\nu\nu b\bar{b}$ single tag (ST) and double tag (DT) channels. Systematic uncertainties are listed by name; see the original references for a detailed explanation of their meaning and on how they are derived. Uncertainties are relative, in percent on the event yield. Shape uncertainties are labeled with an “(S)”, and “SO” represents shape only uncertainty.

$\nu\nu b\bar{b}$ Single Tag (ST) channels relative uncertainties (%)

Contribution	Top	$V + b\bar{b}/c\bar{c}$	$V+l.f.$	Dibosons	Multijet
Jet ID efficiency (S)	2.0	2.0	2.0	2.0	–
Jet Energy Scale (S)	2.2	1.6	3.1	1.0	–
Jet Energy Resolution (S)	0.5	0.3	0.3	0.9	–
Vertex Conf. / Taggability (S)	3.2	1.9	1.7	1.8	–
b Tagging (S)	1.1	0.8	1.8	1.2	–
Lepton Identification	1.6	0.9	0.8	1.0	–
Trigger	2.0	2.0	2.0	2.0	–
Heavy Flavor Fractions	–	20.0	–	–	–
Multijet model	–	–	–	–	25
Cross Sections	10.0	10.2	10.2	7.0	–
Luminosity	6.1	6.1	6.1	6.1	–
Multijet Normalization	–	–	–	–	–
ALPGEN MLM (S)	–	–	SO	–	–
ALPGEN Scale (S)	–	SO	SO	–	–
Underlying Event (S)	–	SO	SO	–	–
PDF, reweighting (S)	SO	SO	SO	SO	–

$\nu\nu b\bar{b}$ Double Tag (DT) channels relative uncertainties (%)

Contribution	Top	$V + b\bar{b}/c\bar{c}$	$V+l.f.$	Dibosons	Multijet
Jet ID efficiency	2.0	2.0	2.0	2.0	–
Jet Energy Scale	2.1	1.6	3.4	1.2	–
Jet Energy Resolution	0.7	0.4	0.5	1.5	–
Vertex Conf. / Taggability	2.6	1.6	1.6	1.8	–
b Tagging	6.2	4.3	4.3	3.7	–
Lepton Identification	2.0	0.9	0.8	0.9	–
Trigger	2.0	2.0	2.0	2.0	–
Heavy Flavor Fractions	–	20.0	–	–	–
Multijet model	–	–	–	–	25
Cross Sections	10.0	10.2	10.2	7.0	–
Luminosity	6.1	6.1	6.1	6.1	–
Multijet Normalization	–	–	–	–	–
ALPGEN MLM pos/neg (S)	–	–	SO	–	–
ALPGEN Scale (S)	–	SO	SO	–	–
Underlying Event (S)	–	SO	SO	–	–
PDF, reweighting (S)	SO	SO	SO	SO	–

TABLE IV: Systematic uncertainties for the $\ell\ell b\bar{b}$ single tag (ST) and double tag (DT) channels. Systematic uncertainties are listed by name; see the original references for a detailed explanation of their meaning and on how they are derived. Uncertainties are relative, in percent on the event yield. Shape uncertainties are labeled with an “(S)”.

$\ell\ell b\bar{b}$ Single Tag (ST) channels relative uncertainties (%)						
Contribution	Multijet	$Z+l.f.$	$Z + b\bar{b}$	$Z + c\bar{c}$	Dibosons	Top
Jet Energy Scale (S)	–	3.0	8.4	10	3.3	1.5
Jet Energy Resolution (S)	–	3.9	5.2	5.3	0.04	0.6
Jet ID efficiency (S)	–	0.9	0.6	0.2	1.0	0.3
Taggability (S)	–	5.2	7.2	7.3	6.9	6.5
Z_{p_T} Model (S)	–	2.7	1.4	1.5	–	–
HF Tagging Efficiency (S)	–	–	5.0	9.4	–	5.2
LF Tagging Efficiency (S)	–	73	–	–	5.8	–
ee Multijet Shape (S)	53	–	–	–	–	–
Multijet Normalization	20-50	–	–	–	–	–
Z +jets Jet Angles (S)	–	1.7	2.7	2.8	–	–
AlpGen MLM (S)	–	0.3	–	–	–	–
AlpGen Scale (S)	–	0.4	0.2	0.2	–	–
Underlying Event (S)	–	0.2	0.1	0.1	–	–
Trigger (S)	–	0.03	0.2	0.3	0.3	0.4
Cross Sections	–	–	20	20	7	10
Normalization	–	1.3	1.3	1.3	8.0	8.0
PDFs	–	1.0	2.4	1.1	0.7	5.9

$\ell\ell b\bar{b}$ Double Tag (DT) channels relative uncertainties (%)						
Contribution	Multijet	$Z+l.f.$	$Z + b\bar{b}$	$Z + c\bar{c}$	Dibosons	Top
Jet Energy Scale (S)	–	4.0	6.4	8.2	3.8	2.7
Jet Energy Resolution(S)	–	2.6	3.9	4.1	0.9	1.5
JET ID efficiency (S)	–	0.7	0.3	0.2	0.7	0.4
Taggability (S)	–	8.6	6.5	8.2	4.6	2.1
Z_{p_T} Model (S)	–	1.6	1.3	1.4	–	–
HF Tagging Efficiency (S)	–	–	1.3	3.2	–	0.7
LF Tagging Efficiency (S)	–	72	–	–	4.0	–
ee Multijet Shape (S)	59	–	–	–	–	–
Multijet Normalization	20-50	–	–	–	–	–
Z +jets Jet Angles (S)	–	2.0	1.5	1.5	–	–
AlpGen MLM (S)	–	0.4	–	–	–	–
AlpGen Scale (S)	–	0.2	0.2	0.2	–	–
Underlying Event(S)	–	0.1	0.02	0.1	–	–
Trigger (S)	–	0.3	0.2	0.1	0.2	0.5
Cross Sections	–	–	20	20	7	10
Normalization	–	1.3	1.3	1.3	8.0	8.0
PDFs	–	1.0	2.4	1.1	0.7	5.9

TABLE V: The correlation matrix for the analysis channels. Uncertainties marked with an \times are considered 100% correlated across the affected channels. Otherwise the uncertainties are not considered correlated, or do not apply to the specific channel. The systematic uncertainties on the background cross section (σ) and the normalization are each subdivided according to the different background processes in each analysis.

Source	$lv\bar{b}\bar{b}$	$\nu\nu\bar{b}\bar{b}$	$ll\bar{b}\bar{b}$
Luminosity	\times	\times	
Normalization			
Jet Energy Scale	\times	\times	\times
Jet ID	\times	\times	\times
Electron ID/Trigger	\times	\times	\times
Muon ID/Trigger	\times	\times	\times
b -Jet Tagging	\times	\times	\times
Background σ	\times	\times	\times
Background Modeling			
Multijet Background			
Signal σ	\times	\times	\times

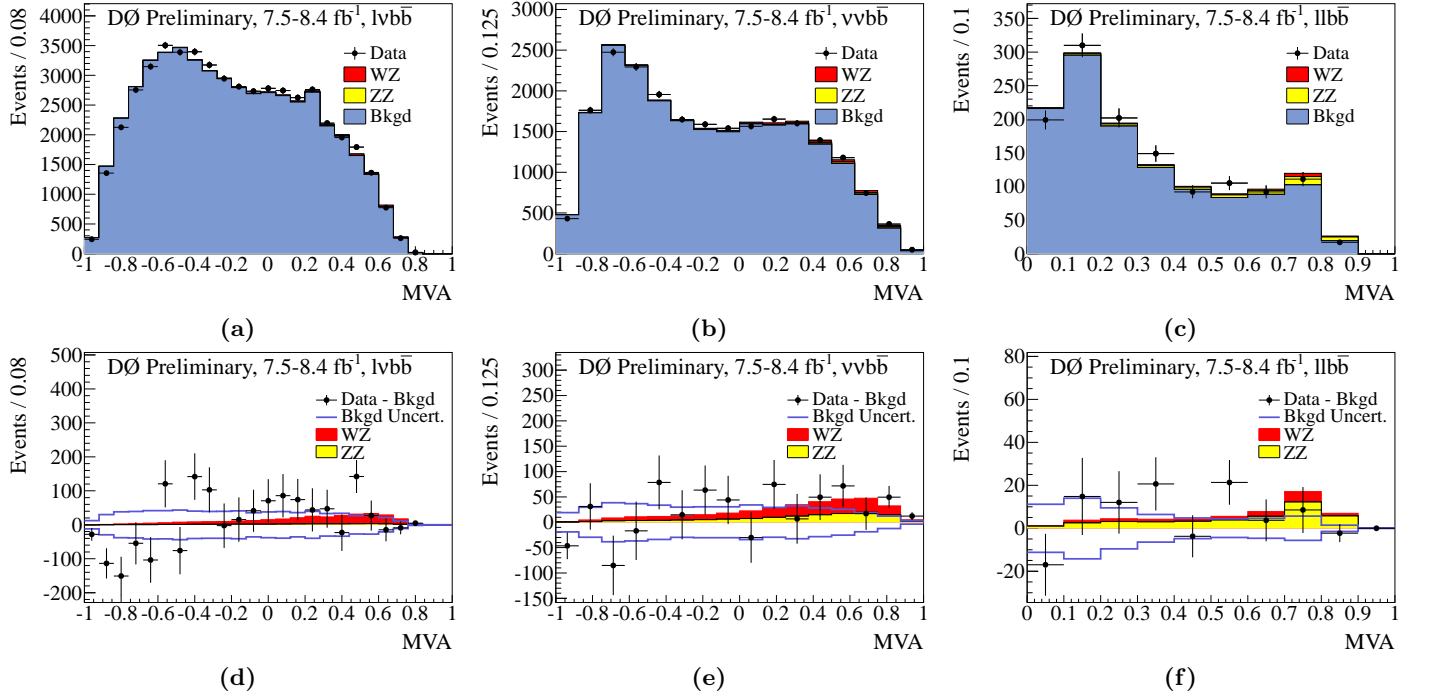


FIG. 7: Comparison of fitted signal+background to the data in the final MVA distributions for the (a) $lv\bar{b}\bar{b}$ (b) $\nu\nu\bar{b}\bar{b}$ and (c) $ll\bar{b}\bar{b}$ analyses (each summed over all sub-channels); and comparison of the measured signal to the background-subtracted data in the (d) $lv\bar{b}\bar{b}$ (e) $\nu\nu\bar{b}\bar{b}$ and (f) $ll\bar{b}\bar{b}$ analyses. The background has been fit to the data in the hypothesis that both signal and background are present. Also shown is the ± 1 standard deviation uncertainty on the fitted background.

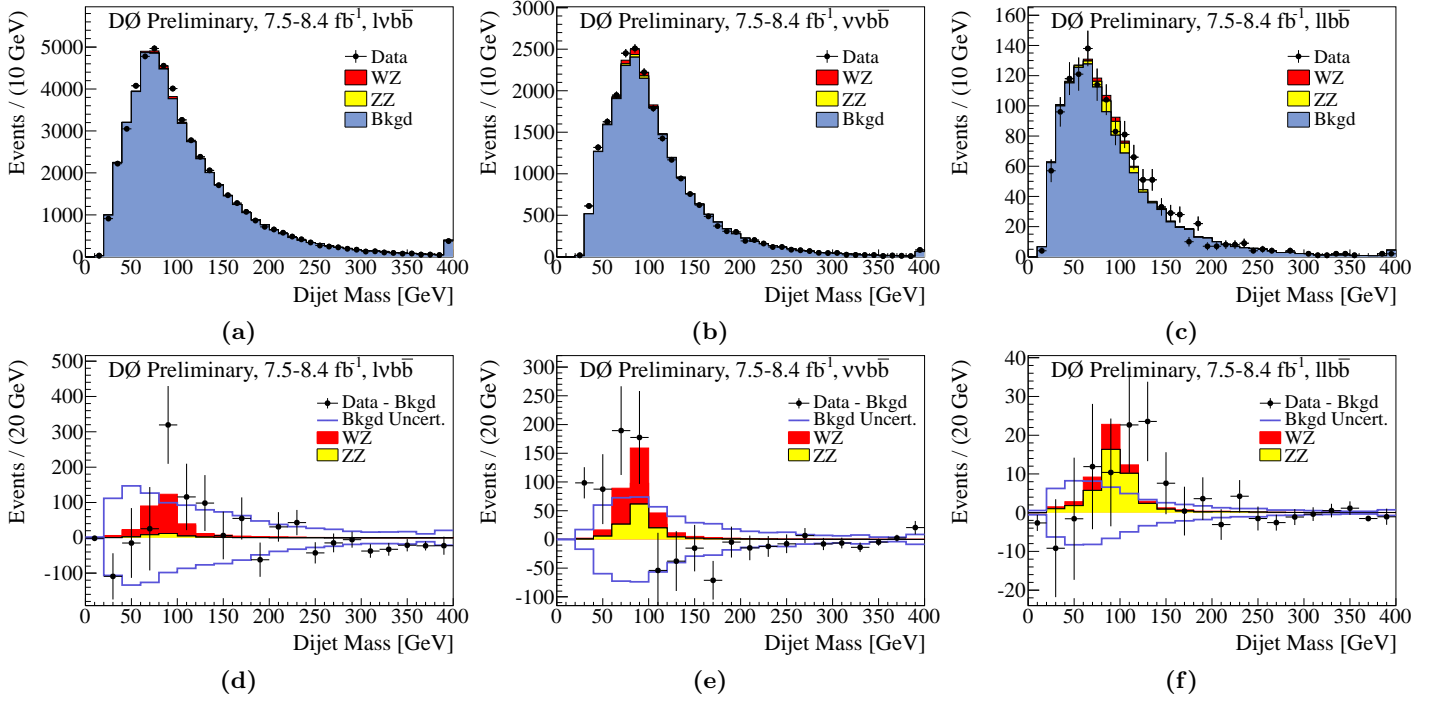


FIG. 8: Comparison of fitted signal+background to the data in the dijet mass distributions for the (a) $\ell\nu b\bar{b}$ (b) $\nu\nu b\bar{b}$ and (c) $\ell\ell b\bar{b}$ analyses (each summed over all sub-channels); and comparison of the measured signal to the background-subtracted data in the (d) $\ell\nu b\bar{b}$ (e) $\nu\nu b\bar{b}$ and (f) $\ell\ell b\bar{b}$ analyses. The background has been fit to the data in the hypothesis that both signal and background are present. Also shown is the ± 1 standard deviation uncertainty on the fitted background. Events with a dijet mass greater than 400 GeV are included in the last bin of the distribution.